MAGNETIC ANALYSIS OF ANTARCTIC ORDINARY CHONDRITES AND ACHONDRITES ON THE BASIS OF A MAGNETIC BINARY SYSTEM MODEL

Takesi Nagata and Minoru Funaki

National Institute of Polar Research, 9–10, Kaga 1-chome, Itabashi-ku, Tokyo 173

Abstract: Magnetic hysteresis cycles of 9 ordinary chondrites and 10 achondrites, collected mainly from Antarctica, are analyzed on the basis of a newly proposed model of a non-interactive magnetic binary system, by taking into account their thermomagnetic characteristics for identifying ferromagnetic phases involved. All the chondrites and achondrites examined consist of a high-coercivity (a) component and a low-coercivity (b) component.

In ordinary chondrites, the (a) component is often identified to be tetrataenite (tetragonal-ordered crystal of FeNi) having an apparent coercive force $H_C^{(a)} \gtrsim 10^3$ Oe (TT-type phase), while in other chondrites the (a) component comprises fine grains of shape-anisotropic single-domain structure (A. SD-type phase) having $H_C^{(a)} = (2\sim5)\times10^2$ Oe. The (b) component consists of mostly multi-domain grains of kamacite and/or taenite of $H_C^{(b)} \lesssim 20$ Oe.

In most achondrites, the (a) component comprises A. SD-type phase of $H_C^{(a)} = (2\sim5)\times10^2$ Oe except a special case consisting of a small amount of tetrataenite. The structure of the (b) component in achondrites is the same as in ordinary chondrites.

An anomalous hump-shape rise in saturation magnetization (I_s) between 330°C and Curie point of taenite ($540\sim590$°C) during the initial heating process is found in diogenites and a eucrite. The thermomagnetic hump is considered here to be due to an increase of A. SD-type phase of taenite associated with a relatively smaller increase of the (b) component multi-domain phase. However, a possible metallographical interpretation of the hump phenomenon has not yet been obtained.

1. Introduction

Magnetic characteristics of ordinary chondrites and achondrites are substantially different from those of terrestrial rocks, because the ferromagnetic constituents of the stone meteorites are mostly Fe-Ni metallic grains present as several distinctly different phases such as kamacite, (ordinary) taenite, tetrataenite (FeNi), awaruite (FeNi$_3$) and metastably ordered kamacite (Fe$_3$Ni), and frequently these phases are not in equilibrium in these meteorites.

On the other hand, the natural remanent magnetization (NRM) of various kinds of meteorites is generally believed to be a record of the magnetic field associated with the primordial solar nebula, in which the meteorite was formed. The NRM of meteorites is very likely either the thermoremanent magnetization (TRM) or the crystalline

(or chemical) remanent magnetization (CRM) acquired in the ambient magnetic field.

Since magnetic characteristics of stone meteorites are substantially different from those of terrestrial rocks, an appropriate physical model, which can reasonably approximate the essential elements of the basic magnetic properties of stone meteorites, will be required for the purpose of estimating the assumed primordial solar nebula magnetic field from experimentally observed data of NRM of the stone meteorites.

In most cases of terrestrial igneous and thermal-metamorphic rocks, a relatively simple model, where fine ferromagnetic particles are uniformly dispersed in a non-magnetic matrix, seems to well approximate physical characteristics of their NRM as identical to their TRM which was acquired during their cooling process in an ambient magnetic field. Actually experimental simulations to produce TRM on terrestrial igneous and thermal-metamorphic rocks are repeatable at least several times and the thermal demagnetization characteristics of the TRM thus produced are satisfactorily same as those of NRM in most cases.

In the case of stone meteorites, however, such a simulation experiment for thier NRM characteristics is often unsatisfactory, the thermal demagnetization characteristics of their TRM being considerably different from those of their NRM. The observed differences are sometimes due to a phase change of the original NRM-bearing ferromagnetic phase, or due to a difference of a main TRM-acquiring component from the main NRM-bearing component.

The magnetic constituents in stone meteorites must be generally considered to consist of two or more different phases, when we are concerned with their NRM characteristics. This implication may be a fairly natural suggestion, if the complexity of coexisting various different phases of Fe-Ni alloys in the lower temperature range is taken into consideration.

From another viewpoint that the ratio of remanence coercive force (H_{RC}) to coercive force (H_C) in the magnetic hysteresis curves of stone meteorites is, in general, anomalously large in comparison with H_{RC}/H_C values of terrestrial igneous and metamorphic rocks, NAGATA and CARLETON (1987) have proposed a non-interactive magnetic binary system model as a simplest possible basic model for the magnetic structure of stone meteorites. It is assumed in their binary system model that high magnetic coercivity particles (a) and low magnetic coercivity particles (b) are dispersed at random in a nonmagnetic matrix and the magnetic interaction among individual particles is negligibly small. Analyses of the magnetic hysteresis loops before and after heat treatments of Antarctic chondrites with the aid of the binary system model have reasonably well verified that a number of chondrites contain a certain amount of tetrataenite of a high magnetic coercivity in addition to a low coercivity metallic particles such as kamacite or ordinary taenite (NAGATA, 1988).

The present work is a continuation of the magnetic analysis of ordinary chondrites and achondrites with the aid of the same magnetic binary system model.

2. Magnetic Analysis of Ordinary Chondrites and Achondrites with the Aid of a Magnetic Binary System Model

Figure 1 illustrates an example of the first-run thermomagnetic curves of an
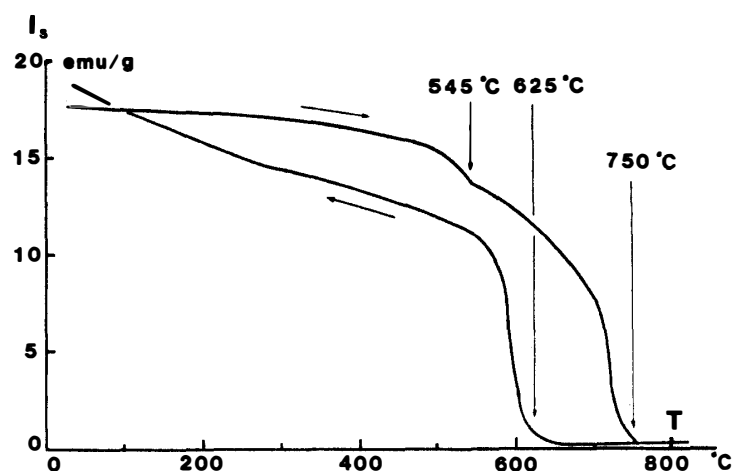
Fig. 1.   The first-run thermomagnetic cycle curve of Y-74354 L6 chondrite.   ($H_{ex}=10\ kOe$).

Antarctic L6 chondrite, Y-74354 (NAGATA and FUNAKI, 1981). On the basis of the observed thermomagnetic characteristics, it has been concluded that the ferromagnetic constituent in this chondrite is mainly composed of a kamacite phase of 6.1 wt% Ni, which is represented by the $\alpha \rightarrow \gamma$ transition at 750°C in the heating curve and the $\gamma \rightarrow \alpha$ transition at 625°C in the cooling curve, and a taenite phase of around 40 wt% Ni, which is represented by an irreversible transition at 545°C in the initial heating curve. This result indicates that the ferromagnetic component of Y-74354 chondrite consists of two major phases, kamacite and taenite. As generally summarized (*e.g.*, NAGATA, 1979), it seems very likely that the structure of metallic grains in chondrites is represented by the co-existence of a Ni-poor Fe-Ni metal and a Ni-rich Fe-Ni metal in most cases.

On the other hand, the proposed magnetic binary system model (NAGATA and CARLETON, 1987) is primarily concerned with the coexistence of a magnetically high coercivity component (a) and a low coercivity component (b). The high coercivity component (a) is represented by uniaxially anisotropic grains such as single crystals of a high crystalline anisotropy or single domain particles having a considerably large shape anisotropy, while the low coercivity component (b) is represented by multi-domain particles having comparatively small crystalline anisotropy. According to the binary system model, the ratio of saturated IRM (I_R) to saturation magnetization (I_S) of a binary system model rock is uniquely dependent on content (m) of the (a)-component in the magnetic constituent. Figure 2 is a diagram of the dependence of I_R/I_S on m for a model system approximating the average magnetic structure of chondritic meteorites, in which are assumed $I_S^{(a)}=160$ emu/g and ($I_R^{(a)}/I_S^{(a)}$)=0.5 for the uniaxially anisotropic high coercivity component (a) and $I_S^{(b)}=210$ emu/g and $I_R^{(b)}/I_S^{(b)}=0.003$ for the multi-domain low coercivity component (b) (NAGATA and CARLETON, 1987; NAGATA, 1988). From an observed value of I_R/I_S of a chondritic meteorite, the m value of its magnetic constituent can be estimated.

Figure 3 illustrates the dependence of coercive force (H_C) and remanence coercive force (H_{RC}) on m for the same model system for an example case that $H_C^{(a)}=1200$ Oe and $H_C^{(b)}=10$ Oe, where $H_{RC}^{(a)}/H_C^{(a)}=1.5$ for the uniaxially anisotropic grains and
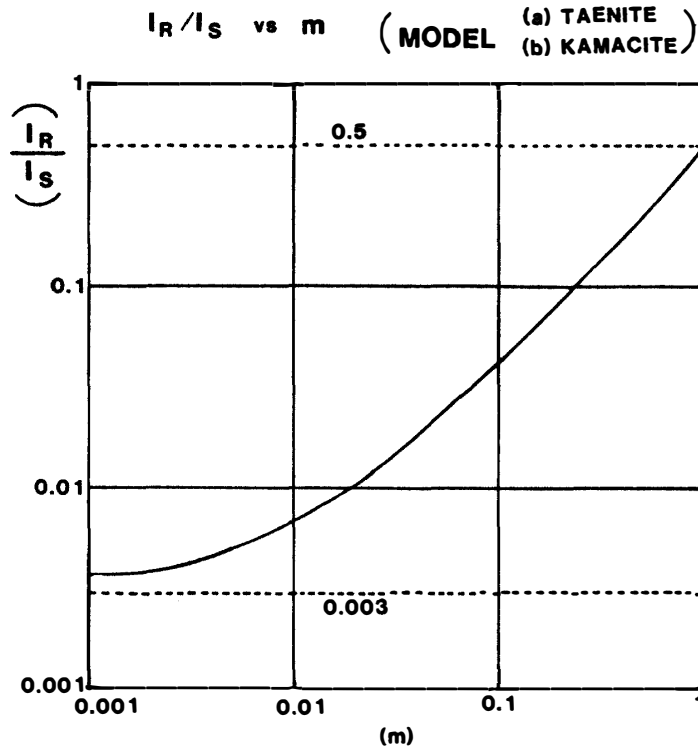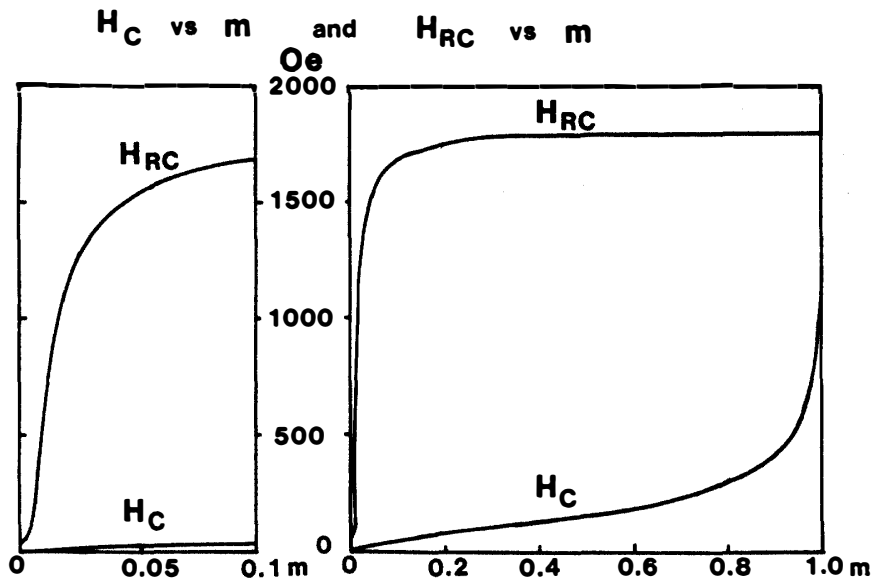
I_R / I_S vs   m $\left(\text{MODEL} \begin{array}{l} \text{(a) TAENITE} \\ \text{(b) KAMACITE} \end{array} \right)$

Fig. 2.   Dependence of ratio of observed values (I_R/I_S) on weight content (m) of a high coercivity
(a)component in the total metal in the standard binary system model for ordinary chondrites
and achondrites.   (See text).

H_C vs   m   and H_{RC} vs   m

MODEL $\left\{ \begin{array}{l} H_C^{(a)} = 1200 \text{ Oe}, \quad H_{RC}^{(a)} = 1800 \text{ Oe}, \\ H_C^{(b)} = \quad 10 \text{ Oe}, \quad H_{RC}^{(b)} = \quad 40 \text{ Oe}, \end{array} \right.$ $\left\{ \begin{array}{l} I_R^{(a)} / I_S^{(a)} = 0.5 \quad \text{(S.D.)} \\ I_R^{(b)} / I_S^{(b)} = 0.003 \text{ (M.D.)} \end{array} \right.$

$I_S^{(a)} = 160$ emu/g (Taenite). $I_S^{(b)} = 210$ emu/g (Kamacite)

Fig. 3.   (Right) Examples of dependence of H_C and H_{RC} on m in the standard binary system model
for ordinary chondrites and achondrites.   ($H_C^{(a)} = 1200$ Oe for the assumed (a) component
and $H_C^{(b)} = 10$ Oe for the assumed (b) component.)   (Left) Same diagram as the diagram
on the right-side with 5 times enlarged abscissa scale.

$H_{RC}^{(b)}/H_C^{(b)} = 4$ for the multi-domain (MD) grains are assumed based on experimental evidence as well as a reasonable theoretical background (NAGATA and CARLETON, 1987). As shown in Fig. 3, H_C value decreases sharply with a decrease of m from unity at the beginning but $\partial H_C/\partial m$ becomes much smaller for small values of m, whereas the H_{RC} value remains nearly the same magnitude as $H_{RC}^{(a)}$ in response to a decreasing m from unity to a decimal magnitude. The left-side diagram in Fig. 3 illustrates a behaviour of H_{RC} value approaching toward $H_{RC}^{(b)}$ with a decrease of m from 0.1 to zero. It seems thus that observed anomalously large values of H_{RC}/H_C of chondritic meteorites are reasonably interpreted to be due to the coexistence of (a) high coercivity uniaxially anisotropic grains and (b) low coercivity multi-domain grains.

In the proposed non-interactive binary system model, m, $H_C^{(a)}$, $H_{RC}^{(a)}$, $H_C^{(b)}$ and $H_{RC}^{(b)}$ can be separately estimated, provided that $I_S^{(a)}$, $I_S^{(b)}$, $I_R^{(a)}/I_S^{(a)}$, $I_R^{(b)}/I_S^{(b)}$, $H_{RC}^{(a)}/H_C^{(a)}$ and $H_{RC}^{(b)}/H_C^{(b)}$ are properly chosen. As far as (a)- and (b)-components represent respectively the uniaxially anisotropic grains and the multi-domain grains, $H_{RC}^{(a)}/H_C^{(a)} = 1.5$ and $H_{RC}^{(b)}/H_C = 4$ are generally reasonable values with probable deviations within 20% (e.g., NAGATA, 1988). $I_R^{(a)}/I_S^{(a)} \simeq 0.5$ also is generally considered to be a reasonable value with probable deviations within 10% (e.g., WOHLFARTH, 1963), while $I_R^{(b)}/I_S^{(b)} = 0.002 \sim 0.003$ appears very likely to be applicable to most Fe-Ni metallic MD grains in meteorites and lunar rocks. In case where observed values of m are very small, being 10^{-3} in order of magnitude, an appropriate selection of the assumed value of $I_R^{(b)}/I_S^{(b)}$ is very critical in evaluating the final binary system model, but an assumption of $I_R^{(b)}/I_S^{(b)} = 0.003$ could be adopted for most chondritic meteorites, in which observed I_R/I_S values are larger than 0.01 (NAGATA, 1988). A selection of the assumed values of $I_S^{(a)}$ and $I_S^{(b)}$, which are necessary for determining m from an observed value of I_R/I_S, may have to be judged based on an appropriate interpretation of thermomagnetic characteristics of the meteorite sample concerned. In Figs. 2 and 3, the median value of I_S for most frequently observed taenite phase, 160 emu/g, is chosen for $I_S^{(a)}$ and the average value of kamacite phase, 210 emu/g, is chosen for $I_S^{(b)}$, because the high coercivity component (a) in ordinary chondrites is almost certainly attributable to tetrataenite having a large uniaxial anisotropy. When such an identification of $I_S^{(a)}$ and $I_S^{(b)}$ is difficult owing to a lack of reliable evidence in the thermomagnetic characteristics or any other available data, an approximation of $I_S^{(a)} = I_S^{(b)}$ may be better adopted, because m is dependent only on I_R/I_S, $I_R^{(a)}/I_S^{(a)}$ and $I_R^{(b)}/I_S^{(b)}$ and independent of $I_R^{(a)} = I_R^{(b)}$. A deviation of this estimated value of m from its true value is less than 30% for any possible values of $I_S^{(a)}$ or $I_S^{(b)}$ in a range between 160 emu/g and 210 emu/g provided $I_R/I_S \gtrsim 0.01$.

In the following, magnetic structures of Antarctic ordinary chondrites and achondrites are analyzed using the above-mentioned guiding principles which are the basis of the proposed non-interactive magnetic binary system model (NAGATA and CARLETON, 1987). In practical experimental procedures, (1) a complete magnetic hysteresis curve at atmospheric temperature, (2) the first-run thermomagnetic cycle curves in 10 kOe magnetic field, (3) a magnetic hysteresis curve after the first heating, (4) the second-run thermomagnetic cycle curves, and (5) a magnetic hysteresis curve after the second heating are successively recorded for each stone meteorite sample.

3. Magnetic Binary Structure of Ordinary Chondrites

Table 1 gives observed values of the magnetic hysteresis parameters at atmospheric temperature, I_S, I_R/I_S, H_C and H_{RC}/H_C, in the first 4 columns, of 9 ordinary chondrites in the original state before any heating treatment and the same parameters after the second heating up to 800°C, and parameters m, $H_C^{(a)}$ and $H_C^{(b)}$ derived from the magnetic binary system model analysis of each observed data in the last 3 columns, where $H_{RC}^{(a)} = (3/2)H_C^{(a)}$ and $H_{RC}^{(b)} = 4H_C^{(b)}$ in accordance with the assumption in the present model. Table 2 gives the chemical composition of metallic constituents of

Table 1. Magnetic binary system components of ordinary chondrites.

Meteorite		I_S (emu/g)	I_R/I_S	H_C (Oe)	H_{RC}/H_C	m	$H_C^{(a)}$ (Oe)	$H_C^{(b)}$ (Oe)
St. Severin	(B)	2.80	0.1785	520	3.54	0.417	1239	47
(LL6)	(A)	3.95	0.0053	9.5	11.58	0.006	1240	6
Olivenza	(B)	2.70	0.1974	770	4.17	0.457	2160	62
(LL5)	(A)	4.4	0.0034	10	3.40	~0	–	10
Y-7301	(B)	20.2	0.0064	10.5	84.1	0.009	3607	6
(H4)	(A)	17.1	0.0275	55	5.62	0.064	227	15
Y-74647	(B)	35.7	0.0087	17.5	55.1	0.015	1284	9
(H4–5)	(A)	35.8	0.0014	~2	~10	~0	–	~10
Y-74191	(B)	14.3	0.0147	36.5	28.3	0.031	901	14
(L3)	(A)	14.1	0.0064	15	21.8	0.006	975	9
Y-74354	(B)	21.8	0.0326	66	39.7	0.077	1925	15
(L6)	(A)	19.8	0.0043	11	15.1	~0	–	11
Y-74362	(B)	9.5	0.0382	84	23.8	0.093	1401	14
(L6)	(A)	11.4	0.0026	6	40.8	~0	–	6
Y-790250	(B)	1.80	0.0256	77.5	8.03	0.059	465	22
(LL4)	(A)	1.38	0.1500	153.5	2.31	0.355	238	20
Y-790448	(B)	4.8	0.0231	63	10.76	0.052	518	18
(LL3)	(A)	5.5	0.1016	175	2.55	0.245	303	27

(B): Before any heat treatment. (A): After second-run heating up to 800°C.

Table 2. Contents of $Fe°$, $Ni°$ and $Co°$ in metallic constituents in chondrites listed in
Table 1.

Chondrite	$Fe°$	$Ni°$ (wt%)	$Co°$	Total (wt%)
Y-7301 (H4)	7.21 (89.8)	0.77 (9.6)	0.05 (0.6)	8.03 (100)
Y-74647 (H5)	15.45 (89.6)	1.75 (10.2)	0.039 (0.2)	17.24 (100)
Y-74191 (L6)	5.66 (86.5)	0.85 (13.0)	0.032 (0.5)	6.54 (100)
Y-74354 (L6)	6.04 (83.4)	1.16 (16.0)	0.040 (0.6)	7.24 (100)
Y-74362 (L6)	6.65 (85.6)	1.08 (13.9)	0.040 (0.5)	7.77 (100)
Y-790448 (LL6)	1.33 (59.6)	0.90 (40.4)	~0 (~0)	2.23 (100)

After HARAMURA, H., KUSHIRO, I. and YANAI, K. (1983).
Numerical figures in parentheses are weight percentage of $Fe°$, $Ni°$ and $Co°$ in the total metal.

6 chondrites in Table 1, analyzed by HARAMURA et al. (1983) for reference.

Observed data and the results of the binary system model analysis of 2 non-Antarctic chondrites are listed at the top of Table 1. The metallographic structure and magnetic properties of Fe-Ni metallic grains in the two LL chondrites, St. Séverin (LL6) and Olivenza (L5), have been studied in fair detail. Results of Mössbauer spectral analysis have shown that the composition of St. Séverin metal is given by

$$\text{(Tetrataenite): (Disordered Taenite): (Kamacite)}=51:9.5:39.5$$

in weight % (NAGATA et al., 1986), and similarly that of the Olivenza metal is given by

$$\text{(Tetrataenite): (Disordered Taenite): (Kamacite)}=40:15:45$$

in weight % (DANON et al., 1985).

As shown in Table 1, results of the present analysis indicate that the original contents (m) of high coercivity (a)-component are 42 wt% and 46 wt% respectively in the St. Séverin and Olivenza metals. After heating twice up to 800°C, however, m values are reduced practically to zero in both LL chondrites, indicating that the ordered crystal structure of tetrataenite in the original state (B) is irreversibly broken down to disordered ordinary taenite by the thermal annealing at the elevated temperature well beyond the transition temperature (320°C) for the tetrataenite-ordered crystal structure (NAGATA et al., 1986). It will be noted in Table 1 that $H_C^{(a)}$ values in the original state before any heating (B) are larger than 10^3 Oersteds.

Checking I_S, m, $H_C^{(a)}$, and $H_C^{(b)}$ values in the original state before any heating (B) and in the thermally annealed state after the heat treatment (A) of 7 Antarctic chondrites in Table 1, it will be noted that 4 chondrites, Y-74647, Y-74191, Y-74354 and Y-74362, have their magnetic structures very similar to those of the St. Séverin and the Olivenza; namely, their m values in (B)-state are reduced down to practically zero in (A)-state, and their $H_C^{(a)}$ values in (B)-state are $H_C^{(a)} \geq 10^3$ Oe.

This result may strongly suggest that Fe-Ni metallic grains in these 4 Antarctic chondrites contain $100\,m$ wt% of tetrataenite phase in (B)-state.

Dealing with some more details of these tetrataenite-bearing chondrites, it is noted that a small amount of the tetrataenite high coercivity component still remains in (A)-state in both the St. Séverin and Y-74191, where $H_C^{(a)}$ values in (A)-state are nearly the same as those in (B)-state. In the Olivenza and Y-74647, Y-74354 and Y-74362 chondrites, on the other hand, their m values in (A)-state are too small to be quantitatively evaluated by the present binary system analysis method.

Throughout all the 6 ordinary chondrites discussed above, observed values of both I_R/I_S and H_C in (A)-state are remarkably reduced from their original values in (B)-state. The above-mentioned remarkable decrease of the originally existing amount of a high coercivity component of $H_C^{(a)} \geq 10^3$ Oe from (B)-state to (A)-state may represent a case that a high coercivity component (a) is thermally unstable tetrataenite and a low coercivity component (b) is composed of multi-domain grains of kamacite and/or ordinary disordered taenite.

The binary structure of Y-7301 chondrite is somewhat special, its m value in (A)-state becoming about 7 times as large as its original value in (B)-state, though $H_C^{(a)}$ value in (B)-state is so large as about 3600 Oe. In Y-790250 and Y-790448 LL

chondrites too, m values in (A)-state become about 6 times and 5 times, respectively, as large as their original values in (B)-state, though their $H_C^{(a)}$ values are around 500 Oe in (B)-state and $200 \sim 300$ Oe in (A)-state.

Since the coercive force H_C along the major axis of a prolate ellipsoidal shape of a single-domain ferromagnetic particle of J_s in spontaneous magnetization is given as

$$H_C = J_s(N_\perp - N_\|) , \qquad (3\text{-}1)$$

where $N_\|$ and $N_\perp$ denote the demagnetizing factors along the major and minor axes respectively,

$$\bar{H}_C = 0.48 H_C , \qquad (3\text{-}2)$$

which is the average coercive force of a random assembly of such shape-anisotropic single-domain ferromagnetic particles can obtain $H_C^{(a)}$ values of $200 \sim 500$ Oe. An approximate evaluation of $\bar{H}_C$ magnitude of such a case results in a relation between $\bar{H}_C$ and ratio (k) of the major axis length to the minor axis length of the prolate particles as given in the following table:

H_C (Oe)	k	
	kamacite ($J_s = 1700$ emu/cm³)	Taenite ($J_s = 1200$ emu/cm³)
200	1.07	1.10
300	1.11	1.15
500	1.19	1.28

It seems most likely that a probable interpretation of the binary structures and their changes from (B)-state to (A)-state of Y-7301, Y-790250 and Y-790448 chondrites will be as follows:

(i) In Y-7301 chondrite, single-domain particles of disordered taenite of $k \sim 1.1$ in shape anisotropy are newly formed in association with a breakdown of the tetrataenite structure caused by the heat treatments.

(ii) The ferromagnetic constituents in Y-790250 chondrite are mostly taenite, kamacite phase being scarcely detected in the thermomagnetic curves. Single-domain disordered taenite particles of $k \sim 1.3$ occupy about 6 wt% of the metallic constituent of this chondrite in (B)-state. Associated with the heat treatment, single-domain disordered taenite grains of $k \sim 1.1$ are newly formed to occupy about 36 wt% of the total metal in (A)-state.

(iii) According to the thermomagnetic curve of the first-run, metallic constituents of Y-790448 chondrite appear to consist of about 40 wt% of taenite and 60 wt% of kamacite on the average in (B)-state. About 5 wt% of the total metal are of single-domain disordered taenite grains of $k \sim 1.3$ in (B)-state. The heat treatment results in a reformation of single-domain taenite grains of $k \sim 1.15$ up to about 25 wt% of the total metal in the final (A)-state.

Summarizing these results of the present binary system model analysis of metallic constituents of ordinary chondrites, it may be provisionally concluded that almost all ordinary chondrites contain, at least, both a high coercivity component (a) and a

low coercivity component (b). The observed characteristics of the high coercivity component (a) may be classified into two groups, i.e., tetrataenite (T.T.) group and shape-anisotropic single-domain (A.SD) group. It seems likely that a structure change of (T.T.) group caused by the thermal annealing effect is relatively simple; the highly coercive tetrataenite structure is broken down by heating up beyond the transformation temperature to submerge into the disordered taenite phase. On the contrary, effects of the thermal annealing on (A.SD) group appear to be more complicated; a considerably larger amount of the high coercivity shape-anisotropic single-domain particles are newly produced by the heat treatment.

The physical mechanism involved in the formation of the microstructures and their thermal changes may have to be experimentally traced in detail in the future.

Since the present non-interactive magnetic binary system model is based on the assumption that possible interactions among individual grains and among different magnetic phases are neglected, possible physical interpretations of the various observed phenomena may need to take into account the effect of mutual interaction among individual elements.

4. Magnetic Binary Structure of Achondrites

In Table 3, observed values of I_S, I_R/I_S, H_C and H_{RC}/H_C of 5 eucrites, a shergottite and 4 diogenites collected from Antarctica in the original (B)-state and in (A)-state after heating twice up to 800°C are listed in the first 4 columns, and the binary system parameters, m, $H_C^{(a)}$ and $H_C^{(b)}$ obtained by the present analyses are tabulated in the

Table 3. Magnetic binary system components of achondrites.

Meteorite		I_S (emu/g)	I_R/I_S	H_C (Oe)	H_{RC}/H_C	m	$H_C^{(a)}$(Oe)	$H_C^{(b)}$(Oe)
Y-74159	(B)	0.175	0.0543	59.5	6.32	0.103	263	11
(Eu)	(A)	0.171	0.0567	75.5	7.79	0.108	410	13
Y-75011	(B)	0.27	0.0096	20	15.40	0.013	337	10
(Eu)	(A)	0.52	0.0113	32	11.42	0.017	534	14
Y-791186	(B)	0.28	0.1000	32	5.81	0.241	190	4
(Eu)	(A)	0.43	0.1488	160	3.54	0.353	573	17
ALH-76005	(B)	0.170	0.0100	15.5	32.97	0.014	564	7
(Eu)	(A)	0.157	0.0503	56	9.84	0.095	388	10
ALH-77302	(B)	0.028	0.1071	50.5	8.02	0.211	276	6
(Eu)	(A)	0.024	0.1417	58.5	5.74	0.279	227	6
ALH-77005	(B)	0.174	0.1301	37	6.30	0.256	158	4
(Sh)	(A)	0.145	0.1703	50	5.44	0.337	183	4
Y-74013	(B)	0.445	0.0056	17	12.53	0.007	1332	11
(Di)	(A)	0.42	0.0464	120	4.39	0.112	555	25
Y-74037	(B)	0.218	0.0206	73	1.96	0.046	98	33
(Di)	(A)	0.250	0.0580	97	4.33	0.140	292	18
Y-74097	(B)	0.318	0.0126	13	10.77	0.025	193	5
(Di)	(A)	0.435	0.0218	54	6.02	0.049	246	17
Y-74648	(B)	0.20	0.0375	85	6.12	0.089	372	19
(Di)	(A)	0.50	0.2180	225	1.87	0.500	282	28

(B): Before any heat treatment.　(A): After second-run heating up to 800°C.

Table 4. Y-791186 (Eucrite).

Thermal history	I_S (emu/g)	$I/_R I_S$	H_C(Oe)	H_{RC}/H_C	m	$H_C^{(a)}$(Oe)	$H_C^{(b)}$(Oe)
Original	0.28	0.1000	32	5.81	0.2414	190	4
After heating to 350°C	0.32	0.0469	69	4.23	0.1128	205	15
After heating to 490°C	0.62	0.1307	136.5	2.70	0.3103	373	18
After heating to 590°C	0.745	0.1785	172.5	2.37	0.4175	412	19
After heating to 840°C	0.43	0.1488	160	3.54	0.3528	573	17

Table 5. Y-74013 (Diogenite).

Thermal history	I_S (emu/g)	I_R/I_S	H_C(Oe)	H_{RC}/H_C	m	$H_C^{(a)}$(Oe)	$H_C^{(b)}$(Oe)
Original	0.445	0.0056	17	12.53	0.0069	1332	11
After heating to 360°C	0.48	0.0552	72	4.61	0.1335	347	14
After heating to 490°C	0.675	0.1052	133.5	2.43	0.2536	331	21
After heating to 610°C	0.70	0.1379	207.5	1.98	0.3283	415	34
After heating to 860°C	0.42	0.0464	120	4.39	0.1116	555	25

Table 6. St. Séverin Si-rich Matrix (L6).

Thermal history	I_S (emu/g)	I_R/I_S	H_C(Oe)	H_{RC}/H_C	m	$H_C^{(a)}$(Oe)	$H_C^{(b)}$(He)
Original	0.120	0.1750	260	5.04	0.4099	883	23
After heating to 355°C	0.25	0.1800	170	2.45	0.4206	421	19
After heating to 390°C	0.375	0.1627	145	2.71	0.3832	397	16
After heating to 505°C	0.45	0.1556	152.5	2.98	0.3676	460	16
After heating to 565°C	0.58	0.1276	137.5	2.97	0.3051	415	17
After heating to 750°C	0.50	0.0840	165	4.47	0.2035	757	24
After heating to 800°C	0.51	0.0667	130	4.12	0.1617	554	22
After heating to 900°C	0.485	0.0268	35	7.49	0.0619	292	9

last 3 columns. The thermomagnetic curves of the first-run and the second-run of Y-791186 eucrite and Y-74013 diogenite are reproduced in Fig. 4, while those of some other Antarctic achondrites have already been reported; they are those of Y-74159 eucrite (NAGATA, 1980) and Y-75011 eucrite (NAGATA and FUNAKI, 1984), and in addition the thermomagnetic characteristics of the other eucrites (ALH-76005, ALH-77302 and ALH-77005) are described as very similar to those of Y-75011 eucrite (NAGATA, 1980), which apparently exhibits a nearly reversible cycle of thermomagnetic curve indicating a single kamacite phase.

As shown in Table 3, achondrites also generally have the magnetic binary structure consisting of a low coercivity component (b) of less than 30 Oe in $H_C^{(b)}$ and a high coercivity component (a) of several hundreds of Oersted in $H_C^{(a)}$ in their original (B)-state, except in the case of Y-74013 diogenite. It appears very likely in Fig. 4 that the main high coercivity component (a) of $H_C^{(a)} = 1332$ Oe in Y-74013 in (B)-state can be identified to tetrataenite phase of only about 0.7 wt% of the total metal. As in the case of Y-7301 chondrite, the tetrataenite phase may be broken down to disordered taenite, and then an (A.SD) type high coercivity component of the shape-anisotropic single-domain taenite particles of $k \sim 1.3$ may be newly developed up to above 11 wt% of the total metal in (A)-state after the heat treatments.

As for the other 9 Antarctic achondrites, their binary structures in both (B)- and (A)-states are attributable to the (A.SD) type high coercivity fine particles of disordered taenite and/or kamacite. Comparing I_S, m, $H_C^{(a)}$ and $H_C^{(b)}$ of achondrites in (B)-state and their changes from (B)-state to (A)-state in Table 3 with the same parameters and their changes of chondrites in Table 1, it will be noted that no example of the typical tetrataenite-dominant binary system characterized by

$$m(\text{A-state}) \ll m(\text{B-state}) \quad \text{and} \quad H_C^{(a)} \gtrsim 10^3 \text{ Oe}$$

can be pointed out from 10 examined samples of achondrite. This result may suggest that the ordered crystal structure of tetrataenite which can be stable only below 320°C in temperature has been mostly transformed to the ordinary disordered taenite phase in most achondrites because of effective thermal metamorphism of their parent planetesimals.

It will be further noted that a change of m value from (B)-state to (A)-state in eucrites having the (A.SD) type high coercivity component in their original state is relatively small, $m(\text{A-state})/m(\text{B-state})$ ranging between 1.05 and 1.45 for 4 eucrites (Y-74159, Y-75011, Y-791186 and ALH-77302) and ALH-77005 shergottite. This result may suggest that the magnetic properties and structures of eucrites are relatively stable against the thermal agitations in the temperature range concerned here. In particular, analyzed results of Y-74159 eucrite given by $I_S(\text{A-state})/I_S(\text{B-state}) = 0.98$, $m(\text{A})/m(\text{B}) = 1.05$, $H_C^{(a)}(\text{A})/H_C^{(a)}(\text{B}) = 1.56$ and $H_C^{(b)}(\text{A})/H_C^{(b)}(\text{B}) = 1.18$ and those of ALH-77302 eucrite given by $I_S(\text{A})/I_S(\text{B}) = 0.86$, $m(\text{A})/m(\text{B}) = 1.32$, $H_C^{(a)}(\text{A})/H_C^{(a)}(\text{B}) = 0.82$ and $H_C^{(b)}(\text{A})/H_C^{(b)}(\text{B}) = 1$ appear to suggest a possible approximate applicability of the Konigisberger-Thellier technique on these eucrites for the purpose of estimating the paleomagnetic field intensity near the surface of their parent planetesimals on the assumption of the thermoremanent magnetization process for the natural acquisition of their natural remanent magnetization. Experimental and analytical discussions on this paleointensity problem, however, will be dealt with elsewhere.

5. Binary System Model Analysis of Thermomagnetic "Hump" Phenomenon

In Fig. 4, the fist heating thermomagnetic curves of both Y-791186 eucrite and Y-74013 diogenite exhibit a "hump" shape rise between 330°C and about 550°C in an external magnetic field of 10 kOe in intensity. On the first-run cooling thermomagnetic curve and on the second-run heating and cooling thermomagnetic curves,

the hump shape rise does not take place, but the ordinary Curie point transition of taenite phase magnetization is observed. Since the observed thermomagnetic curves are substantially equal to the thermal change of saturation magnetization (I_S), the observed hump-shape rise of I_S should be distinguished from a sharp rise of magnetic susceptibility, which frequently takes place at temperatures a little below Curie point (i.e., the so-called Hopkinson effect), because the Hopkinson effect can be physically interpreted as due to a sharp decrease of I_S toward zero. The observed hump-shape rise of I_S will be therefore provisionally called "thermomagnetic hump" here. A similar thermomagnetic hump takes place on the first-run heating thermomagnetic curves of Y-74037, Y-74097 and Y-74648 diogenites, too.

As illustrated in Fig. 5, a sharp thermomagnetic hump is observed on the first-run thermomagnetic curve of silicate-rich matrix of St. Séverin LL6 chondrite, the bulk metallic component of which contains tetrataenite phase of about 40 wt%. In this case also, the thermomagnetic hump does not take place on the first-run cooling thermomagnetic curve and thereafter.

Since the observed thermomagnetic hump phenomenon of I_S is considered to be caused by a certain change in the magnetic composition and structure of ferromagnetic Fe-Ni metals in the stone meteorites with increasing temperature, their magnetic hysteresis characteristics at atmospheric temperature after heating up to successively increasing temperatures are subjected to the present magnetic binary system model analysis. Tables 4, 5 and 6 show the observed magnetic hysteresis parameters, I_S, I_R/I_S, H_C and H_{RC}/H_C in the original state and after heating up to designated temperatures, and the binary structure parameters, m, $H_C^{(a)}$ and $H_C^{(b)}$ obtained by the analysis for Y-791186 eucrite, Y-74013 diogenite and St. Séverin matrix, respectively. In all the three cases, I_S value begins to increase by heating to about 350°C, approaches nearly the maximum value by heating to about 500°C and completes the increasing tendency of I_S value by heating to about 600°C, then I_S value being reduced by heating above 800°C for a thermal annealing.

As already discussed, the high coercivity component (a) in the original state in both St. Séverin matrix and Y-74013 is considered to be composed mostly of tetrataenite, but it seems very likely that the tetrataenite phase is broken down at temperatures below 360°C to fine grains of disordered taenite of (A.SD) type. It will be considered, on the contrary, that the high coercivity component (a) in Y-791186 in the original state and through all the heated states is shape-anisotropic fine grains of (A.SD) type.

As indicated by changes of m values within a heating temperature range from about 350°C to 600°C for Y-791186 and Y-74013, the relative content of the high coercivity (A.SD) type component also increases, together with an increase of I_S, with increasing temperature within a 350~600°C range. In contrast to these two cases, m value of St. Séverin matrix after the breakdown of tetrataenite phase decreases monotonously with an increase of the annealing temperature, regardless of an increase of I_S value with the same heat treatments.

For the purpose of examining more in detail of the observed changes of I_S and m caused by the thermal annealing, the bulk contents of the high coercivity component (a), $m(a)$, and the low coercivity component (b), $m(b)$, are evaluated for each annealing

temperature.   The bulk contents, m(a) and m(b), are given by

$$m(\text{a})=mI_\text{S}/\{mI_\text{S}^{(\text{a})}+(1-m)I_\text{S}^{(\text{b})}\}\ ,$$

$$m(\text{b})=(1-m)I_\text{S}/\{mI_\text{S}^{(\text{a})}+(1-m)I_\text{S}^{(\text{a})}\}\ .\qquad\qquad(5\text{-}1)$$

As indicated by the thermomagentic curves in Fig. 4, Fe-Ni metals in Y-791186 eucrite are mostly taenite, so that both $I_\text{S}^{(\text{a})}$ and $I_\text{S}^{(\text{b})}$ can take the average value for taenite, i.e. $I_\text{S}^{(\text{a})}=I_\text{S}^{(\text{b})}=160$ emu/g.   The thermomagnetic characteristics of Y-74013 diogenite and St. Séverin matrix, shown in Fig. 4 and Fig. 5 respectively, may suggest that the majority of the low coercivity component (b) in these two specimens are kamacite multi-domain grains of $H_\text{C}^{(\text{b})}\lesssim20$ Oe, so that $I_\text{S}^{(\text{a})}=160$ emu/g and $I_\text{S}^{(\text{b})}=210$ emu/g may be assumed as reasonable approximate values.   In any case, m(a) and m(b) are not seriously sensitive to the assumed values of $I_\text{S}^{(\text{a})}$ and $I_\text{S}^{(\text{b})}$ as far as these values are between 160 emu/g and 210 emu/g.   Diagrams of m(a) versus m(b) thus obtained for each state after the successive heatings of the three specimens are illustrated in Fig. 6, where general characteristics of the m(a) versus m(b) diagrams are similar to each other for Y-791186 and Y-74013, but those of St. Séverin matrix are considerably different from the two diagrams of Antarctic achondrites.   Corresponding to the thermomagnetic humps of Y-791186 and Y-74013, m(a) after heating approximately to 600°C is enlarged to (4~8) times as large as its initial value after heating to about 350°C, while m(b) becomes only (1.2~1.5) times as large as its initial value for the same heat treatments, and both m(a) and m(b) tend to return to their original values after a considerably effective thermal annealing by heating twice to temperatures above 800°C.   In contrast with the growth and reduction behaviors of m(a) and m(b) of the two achondrites, m(a) and m(b) values of St. Séverin matrix specimen increase about 1.6 times and about 3 times, respectively, as large as their initial values in association with its thermomagnetic hump, and only m(a) is considerably reduced while m(b) is kept practically invariant by the effective thermal annealing at temperatures above 800°C.

From the experimental results expressed in terms of the magnetic binary system model parameters in Fig. 6, it may be phenomenologically concluded that the thermomagnetic hump phenomenon observed with Antarctic achondrites may probably be caused by fine (A.SD) type shape-anisotropic grains of taenite whose Curie point is 540~565°C, with an associated increase of the low coercivity multi-domain particles of taenite and/or kamacite.   A significant problem concerned with the thermomagnetic hump phenomenon of achondrites may be a possible interpretation of the initial rise starting temperature of a thermomagnetic hump at about 330°C.   In connection with this problem, a thermomagnetic hump-shape rise phenomenon of an extracted silicate-rich matrix powder assembly of St. Séverin chondrite has been specifically examined in some detail, because Fe-Ni metallic fine grains in this achondrite-like specimen certainly contain the tetrataenite phase which has its order-disorder transformation temperature at 320°C.   As illustrated in Figs. 4, 5 and 6, some similarity can be pointed out between the thermomagnetic hump of achondrites and that of St. Séverin matrix powder assembly.   However, phenomenological behaviours of a formation of a hump on the thermomagnetic curve of achondrites may not be exactly identified to
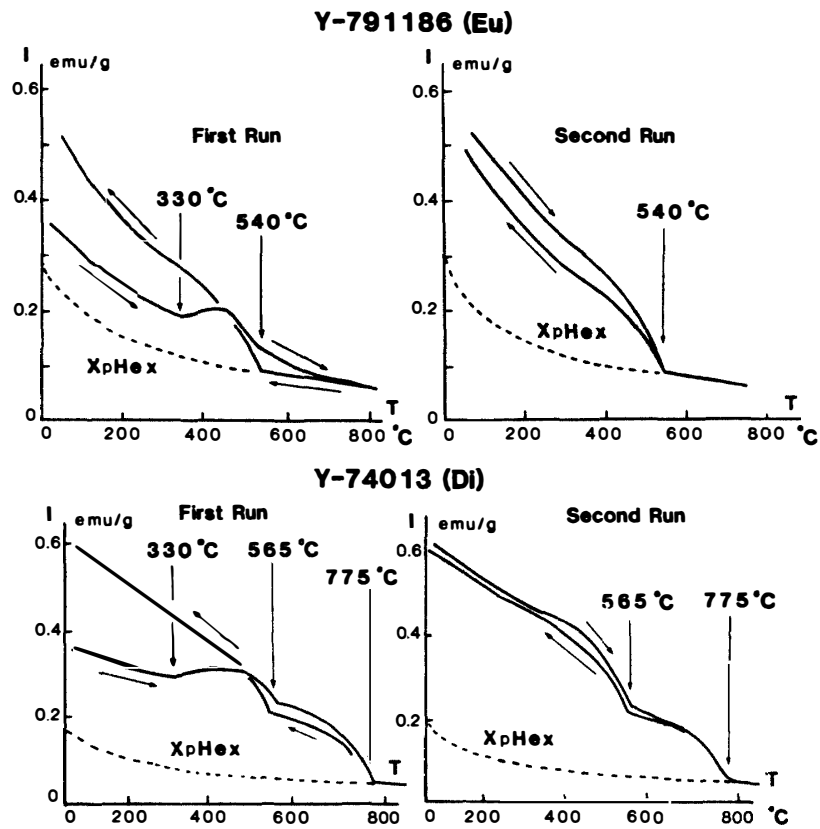
Y-791186 (Eu)

Y-74013 (Di)

Fig. 4. (Top) Thermomagnetic cycle curves of Y-791186 eucrite, showing a thermomagnetic hump rise on the first-run heating curve. ($H_{ex}=10$ kOe.) (Bottom) Thermomagnetic cycle curves of Y-74013 diogenite, showing a thermomagnetic hump rise on the first-run heating curve. ($H_{ex}=10$ kOe).
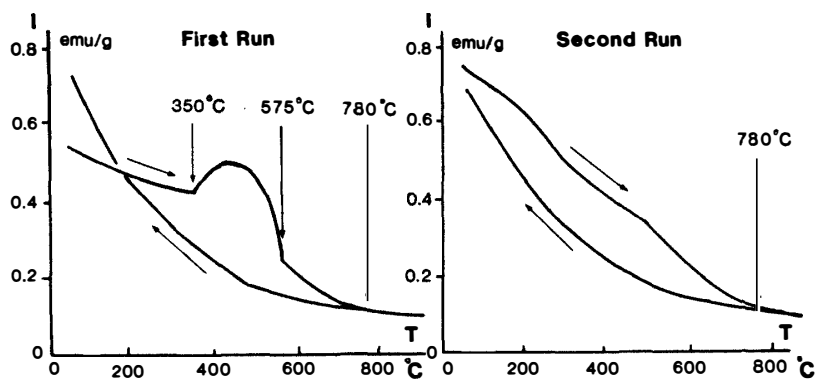

Fig. 5. Thermomagnetic cycle curves of an achondrite-like specimen made of silicate-rich matrix fine grains of St. Séverin LL6 chondrite, exhibiting a thermomagnetic hump rise on the first-run heating curve. ($H_{ex}=10$ kOe).

those of St. Séverin matrix specimen. In future studies on a possible mechanism of the formation process of a thermomagnetic hump in achondrites as well as St. Séverin silicate-rich matrix specimen, direct metallographical examinations of the micro-structures of individual Fe-Ni metallic grains at each annealed state will be required.
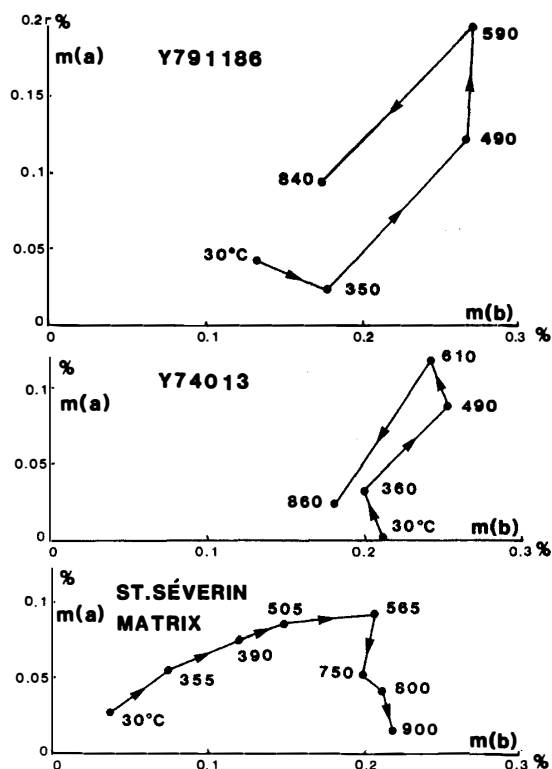
Fig. 6. m (a) versus m (b) diagrams for Y-791186 eucrite (top), Y-74013 diogenite (middle) and St. Séverin silicate-rich matrix (bottom). m(a)+m(b) of each plot gives the content of total Ni-Fe metal in the bulk composition.

6. Concluding Remarks

Results of the present magnetic analyses of Antarctic ordinary chondrites and achondrites on the basis of non-interactive binary system model as well as their thermomagnetic characteristics may have revealed, to a certain extent, the inner structure of ferromagnetic Fe-Ni metallic grains contained in these stone meteorites. It seems likely, for instance, that the thermal destruction of the ordered tetrataenite phase which is fairly commonly present in ordinary chondrites is well demonstrated with the aid of the present method of analysis, even though a certain presence of an interaction effect among ferromagnetic particles is ignored.

As clearly stated in the form of a summary by WOHLFARTH (1963), it is hardly possible to theoretically take into account, in general, the effect of interaction among all elemental magnetic particles forming an assembly, but a certain reasonable semi-quantitative approximation method of analysis for the interaction effect may have to be introduced, case by case, to understand observed magnetic properties and behaviour of various meteorites. For example, $H_C^{(a)}$ values of the (a) component identified to tetrataenite phase are ranged from 900 Oe to 3600 Oe in Table 1. In regard to this problem, various possible configuration patterns of neighbouring ferromagnetic materials around a high coercivity particle to result in a reduction of its apparent H_C value have already been pointed out for observed examples of terrestrial rocks (*e.g.*, NAGATA, 1961). For further research in detail of magnetic structures and properties of meteorites, including a problem of the thermomagnetic hump phenomenon, aids of extended microscopic analyses of ferromagnetic mineral grains in meteorites by the use of microanalyzers of a high magnification and a high precision will be required.

Acknowledgments

References

DANON, J., FUNAKI, M. and NAGATA, T. (1985): Mössbauer spectrum and magnetic properties of the Olivenza chondrite. Meteoritics, 20, 349.

HARAMURA, H., KUSHIRO, I. and YANAI, K. (1983): Chemical composition of Antarctic meteorites, I. Mem. Natl Inst. Polar Res., Spec. Issue, 30, 109–121.

NAGATA, T. (1961): Rock Magnetism (rev. ed.). Tokyo, Maruzen, 350 p.

NAGATA, T. (1979): Meteorite magnetism and the early solar system magnetic field. Phys. Earth Planet. Int., 20, 324–341.

NAGATA, T. (1980): Magnetic classification of Antarctic achondrites. Mem. Natl Inst. Polar Res., Spec. Issue, 17, 219–232.

NAGATA, T. (1988): Magnetic analysis of Antarctic chondrites on the basis of magnetic binary system model, Proc. NIPR Symp. Antarct. Meteorites, 1, 247–260.

NAGATA, T. and CARLETON, B. J. (1987): Magnetic remanence coercivity of rocks. J. Geomag. Geoelectr., 39, 447–461.

NAGATA, T. and FUNAKI, M. (1981): Magnetic properties of Antarctic stony meteorites, Yamato-74115 (H5), -74190 (L6), -74354 (L6), -74362 (L6) and -74646 (LL6). Mem. Natl Inst. Polar Res., Spec. Issue, 20, 316–332.

NAGATA, T. and FUNAKI, M. (1984): Notes on magnetic properties of Antarctic polymict eucrites. Mem. Natl Inst. Polar Res., Spec. Issue, 20, 319–326.

NAGATA, T., FUNAKI, M. and DANON, J. A. (1986): Magnetic properties of tetrataenite-rich meteorites. II. Mem. Natl Inst. Polar Res., Spec. Issue, 41, 364–381.

WOHLFARTH, P. G. (1963): Permanent magnetic materials. Magnetism Vol. III, ed. by G. T. RADO and H. SUHL. New York, Academic Press, 351–393.